Metal nanoparticles embedded in cellulose nanocrystal based films: material properties and post-use analysis

Erlantz Lizundia[1,2], Uribarri Goikuria[2], José Luis Vilas[2,3], Francesco Cristofaro[4,5], Giovanna Bruni[6], Elena Fortunati[7], Ilaria Armentano[8*], L. Visai[4,5], L. Torre[7]*

[1] Dept. of Graphic Design and Engineering Projects. Bilbao Faculty of Engineering. University of the Basque Country (UPV/EHU), Bilbao 48013, Spain.

[2] Macromolecular Chemistry Research Group. Dept. of Physical Chemistry. Faculty of Science and Technology. University of the Basque Country (UPV/EHU), Leioa 48940, Spain.

[3] Basque Center for Materials, Applications and Nanostructures (BCMaterials), Parque Tecnológico de Bizkaia, Ed. 500, 48160 Derio, Spain.

[4] Molecular Medicine Department (DMM), Center for Health Technologies (CHT), UdR INSTM, University of Pavia, Via Taramelli 3/B, 27100 Pavia, Italy

[5] Department of Occupational Medicine, Toxicology and Environmental Risks, Istituti Clinici Scientifici Maugeri S.p.A., IRCCS, Virca S. Boezio, 28, 27100 Pavia, Italy

[6] Department of Chemistry, Section of Physical Chemistry, University of Pavia, Via Taramelli 12, 27100 Pavia, Italy

[7] University of Perugia, Civil and Environmental Engineering Department, UdR INSTM, Strada di Pentima 4, 05100 Terni, Italy.

[8] Department of Ecological and Biological Sciences (DEB), Tuscia University, Largo dell'Università, 01100, Viterbo, Italy

KEYWORDS: cellulose nanocrystal; metallic nanoparticle; nanocomposite; biodegradation; compost disintegrability; antibacterial activity.

ABSTRACT. The dispersion of nanoparticles with different size-, shape-, and composition-dependent properties is a promising approach to design and fabricate functional materials and devices. This paper reports the results of a detailed investigation of the preparation and properties of free-standing nanocomposite films based on cellulose nanocrystals (CNC) loaded with three different types of metal nanoparticles. CNC-based nanocomposites having zinc oxide (ZnO), titanium dioxide (TiO_2) and silver oxide (Ag_2O) have been fabricated by evaporation-induced self-assembly (EISA) using solely water as dispersing agent. Morphological and optical characteristics, chemical properties, wettability and antimicrobial assays of the produced films were conducted. Furthermore, disintegrability in composting condition of CNC based nanocomposites was here investigated for the first time. The morphological observations revealed the formation of a chiral nematic structure with uniformly distributed nanoparticles. The bionanocomposite films based on the metal nanoparticles had effective antimicrobial activity, killing both *Escherichia coli RB* (*E. coli* RB), and *Staphylococcus aureus 8325-4* (*S. aureus* 8325-4). The simplicity of film preparation, the abundance of cellulose nanocrystals, and the free-standing nature of the nanocomposite films offer highly advantageous features and pave the way for the generation of functional materials.

INTRODUCTION

In recent years, the threat of potentially harmful bacteria stresses is increasing the importance in the scientific research of developing new antimicrobial biomaterials to combat human pandemics. Furthermore, to combine the antimicrobial properties with bio-based and degradable materials is an important challenge. Biomaterials with antibacterial properties have ideally to respond to a wide spectrum of infections, with a primary scope to prevent the treatment or the reduction of the infections[1]. In this regard, high antibacterial performance with bactericidal and/or adhesion-resistant properties has been achieved nanostructured materials with antibacterial properties are under exploration[2,3].

Cellulose is one of the excellent natural materials, with wide different applications, due to its good biodegradability, biocompatibility and non-toxicity[4-6], and it could be considered as the major natural and inexhaustible source of raw materials meeting the increasing demand for green and biocompatible products[7]. During the last decade, cellulose-based materials have been proven to be suitable for the development of environmentally-friendly films with potential applications in different field because of their biocompatibility, low cost, and wide availability[8], mainly in combination with other bio-based and/or biodegradable polymer, in order to develop bionanocomposite materials. Cellulosic nanostructures are recognized as innovative nanomaterials which enable the development of new materials with improved performance. In this sense, cellulose nanocrystals (CNC) emerge as one of the most promising form of cellulosic materials for novel applications due to their inherent characteristics. CNC are extracted via controlled disintegration of cellulose, being acid-hydrolysis the most common method[7-9]. As a result of the controlled disintegration of the amorphous and disordered regions of cellulose, well-

defined nanosized crystals having a modulus of elasticity of about 150 GPa and low density of 1.57 g/cm^3 are achieved[10].

Cellulose has been explored as material for nanocomposite development, because of the presence of several functional groups that may be employed in various activation processes. The development of nanocomposites is a common strategy to upgrade the functional properties of the hosting matrix[8,9,11-13]. For example, the addition of nanofillers into several biopolymers has already leaded to improvements in the physico-mechanical performance of their hosting matrices[8,14]. In this framework, the incorporation of metal nanoparticles such as silver, titanium and zinc into a hosting matrix has been proven to efficiently provide antibacterial properties to the whole system at the same time that they provide ultraviolet (UV) screening properties[15-17]. Among the various metal nanoparticles, silver nanoparticles were extensively studied because of their potential antibacterial properties[8,15-17]; nanosized silver particles show both Gram-positive and Gram-negative antimicrobial properties[18]. However, the biomedical applications of silver nanoparticles are potentially limited, due to their genotoxicity towards mammalian cell and their non-specific biological toxicity[19, 20]. Alternatively, zinc oxide (ZnO), an interesting transition metal oxide, is used as an effective entity for devastating the microbial growth. ZnO possesses good catalytic, electrical, photochemical and optical properties, it is used in the area of bioscience as a biomimetic membrane; furthermore it can immobilize and modify proteins because of the fast electron transfer between the enzyme's active sites and the electrode[21]. In addition, ZnO has a lot of advantages: it is non-toxic and chemically stable under exposure to both high temperatures and UV light[22]. The assembly of nanometer-scale building blocks with distinct sizes, shapes, and compositions is a promising approach to the design and fabrication of functional nanocomposite materials with new structures and properties[23]. Fine dispersion of

nanoparticles in a polymer matrix that can permit the functional presence, without the direct contact of the nanoparticles with biological entities is an important challenge. Additionally, from an environmental point of view, it is desirable to sped-up the film disintegration in compost conditions once the films have been used. This modulation of the biodegradation profile could be attempted as well by the introduction of proper nanoparticles into the hosting polymer matrix. Unfortunately, obtaining a homogeneous dispersion of these nanoparticles is not a trivial issue due to their tendency to aggregate thanks to their high surface energy[24]. Several approaches known as grafting from, grafting to and grafting through have been carried out to overcome this issue, although they usually require long and complex chemical processes which are not easily scalable[25]. Moreover, the introduced surfactants when preparing nanocomposites with well-dispersed particles are toxic and not suitable for biomedical applications[26]. Conversely, evaporation-induced self-assembly (EISA) arises as an efficient approach to fabricate CNC-based nanohybrids with randomly distributed nanoparticles because the electrostatic repulsion forces between adjacent CNC (when dispersed in water) keep the individual composite constituents homogeneously distributed in solution at the molecular level[27]. This simple approach is scalable through the existing papermaking technologies, enabling the fabrication of simple formulations for the industry via a cost-effective process.

The aim of this work is to design, synthesize and characterize innovative antibacterial biomaterials based on cellulose nanocrystals and metal nanoparticles and to explore the effect of dimensions, shape and chemistry on final nanocomposite properties, including the disintegration of these materials in composting conditions and their suitability as antimicrobial systems.

MATERIALS AND METHODS

Starting materials

Microcrystalline cellulose with a particle size of 20 µm (310697-500G), sulphuric acid, and sodium hydroxide (NaOH) have been supplied by Sigma Aldrich. The acetone (HPLC grade, assay>99.8 %) was purchased from LabScan, while methanol (reagent ≥ 99.5 %) was purchased by Panreac. ZnO and TiO_2 nanoparticles have been kindly purchased by L´Urederra technological centre (Spain). Ag_2O was provided by Cima NanoTech (Corporate Headquarters, Saint Paul, MN, USA).

Cellulose nanocrystal synthesis

Cellulose nanocrystals (CNC) were obtained by sulphuric acid hydrolysis of microcrystalline cellulose as described previously[28]. Briefly, microcrystalline cellulose was hydrolyzed in a 64 % (w/w) sulphuric acid solution at 45 ºC during 30 min. Hydrolytic reaction was stopped by adding 20-fold distilled water. Hydrolyzed cellulose was recovered after centrifugation (6000 rpm for 10 min) and it was subsequently washed using a Buchner flask and Buchner funnel until neutral pH. Resulting suspension was further neutralized by adding 1% (v/v) 0.25 mol/L of sodium hydroxide (NaOH). Finally, remaining suspension was sonicated at an output of 40 % for 5 min with a Vibracell Sonicator. Cellulose nanocrystals with a zeta potential of -0.6 mV (as measured using a Malvern Zetasizer Nano instrument) have been obtained.

CNC based film fabrication

Mechanically flexible CNC/ZnO, CNC/TiO_2 and CNC/Ag_2O films have been prepared by evaporation-induced self-assembly (EISA), as reported by Lizundia et al.[9]. Metallic

nanoparticles were dispersed in distilled water via mild-sonication (20 % output for 5 min in a Vibra-CellTM CV 334) and they were added to 2.2 wt% aqueous CNC dispersions to yield composite materials having 1 wt% (CNC to metal nanoparticles). Subsequently, another sonication step at 20 % output for further 5 min has been applied to aqueous CNC/ZnO dispersions before casting them in 6x4 cm2 silicone molds. Samples were dried at 35 ºC on a hot plate (RH of 52 %) for 48 h followed by another 24 h at 60 ºC in a vacuum-oven. Neat CNC film was also prepared for comparison. Films with thicknesses of 300 ± 20 μm were obtained.

Thermogravimetric analysis (TGA)

Thermogravimetric analysis (TGA) was performed on 10 mg samples by a Seiko Exstar 6000 TGA quartz rod microbalance. The tests were done under nitrogen atmosphere from 25 to 900ºC at 10ºC/min.

Morphological characterization

Cellulose nanocrystals were examined by transmission electron microscopy (TEM) by using a Philips CM120 Biofilter apparatus with STEM module at an acceleration voltage of 120 kV. CNC-based nanocomposite films have been analyzed in a Hitachi S-4800 field emission scanning electron microscope (FE-SEM) at an acceleration voltage of 15 kV. Analyzed surfaces were copper-coated in a Quorum Q150T ES turbo-pumped sputter coater (5 nm thick coating).

UV-Vis spectroscopy

UV-Vis absorption spectra were recorded by a Shimadzu MultiSpec-1501 spectrophotometer. Total transmittance experiments have been analyzed in the range of 200 to 800 nm with a sampling interval of 1 nm and 25 accumulations.

Contact angle measurements

Milli-Q water was used as probe liquids for the determination of film surface hydrophobicity. Measurements were carried out by sessile drop method (2 µL per drop at a rate of 2 µL/s) using a Neurtek Instruments OCA 15 EC at room temperature. The average values were calculated using six measurements of each composition.

Antibacterial assays

The microorganisms used in this study were *Escherichia coli RB* (*E. coli* RB), and *Staphylococcus aureus* 8325-4 (*S. aureus* 8325-4)[29]. *E. coli* RB was provided by the "Zooprofilattico Institute of Pavia", Italy whereas *S. aureus* 8325-4 were kindly supplied by Timothy J. Foster (Department of Microbiology, Dublin, Ireland). All bacteria strains were routinely grown in their culture medium overnight under aerobic conditions at 37°C using a shaker incubator (New Brunswick Scientific Co., Edison, NJ, USA): *E. coli* RB in Luria Bertani Broth (LB) (Difco, Detroit, MI, USA), and *S. aureus* 8325-4 in Brian Heart Infusion (BHI) (Difco). These cultures were statically incubated at 37°C under aerobic conditions and reduced to a final density of $1x10^{10}$ cells/mL as determined by comparing the optical density (OD_{600}) of the sample with a standard curve relating OD_{600} to cell number.

All types of CNC-based films were previously sterilized (70% ethanol for 10 min, followed by washings with sterile distilled water) and directly incubated with 200 µL $5x10^4$ *S. aureus* or *E.*

coli cell suspensions for 3 and 24h at 37°C, respectively. At the indicated time points, an MTT test was performed both on the planktonic cell cultures after being in contact with the different CNC-based films and on the cells adherent to the surface of materials to determine the number of live cells. The same aliquot of bacteria was cultured and treated in Tissue Culture Plate (TCP). Results were normalized to TCP and expressed as ratio between bacterial surviving fraction on CNC-based films and neat CNC films. The experiments were performed in duplicate and repeated 3 times.

Scanning Electron Microscopy (SEM) observations of bacteria

For morphological evaluation of adherent cells[30], both bacterial suspensions were seeded on either thermanox coverslip (internal control) (NuncTM) placed at the bottom of a 24-well culture plates, on CNC and on all types of CNC films containing metallic nanoparticles. The incubation was performed for both 3 and 24h at 37°C. Following incubation, samples were washed carefully with sterile water and fixed with 2.5% (v/v) glutaraldehyde in 0.1 M Na-cacodylate buffer, pH 7.2 for 1h at +4°C. After additional washing with cacodylate buffer, the samples were dehydrated using increasing concentrations of ethanol (25, 50, 75%) for 5 min and finally with two washes in 96% ethanol for 10 min. The samples were dried to the critical point using an Emitech K-850 apparatus (Emitech, Ashford, Kent, UK) placed on a mounting base and sputter coated with gold. Once prepared, the samples were investigated using a Zeiss EVO-MA10 scanning electron microscope (Carl Zeiss, Oberkochen, Germany). SEM observations were performed at 2 magnifications: 3.000X and 10.000X.

Disintegrability in composting conditions

Disintegration test under composting conditions was carried applying the European standard ISO 20200 (ISO20200 - Determination of the degree of disintegration of plastic materials under simulated composting conditions in a laboratory-scale test). The test was performed at laboratory-scale and determines the degree of disintegration of plastic materials under simulated intensive aerobic composting conditions at 58 ºC and 50% of humidity. The degree of disintegration D was calculated in percent by normalizing the sample weight at different days of incubation to the initial weight by using Equation (1):

$$D = \frac{m_i - m_r}{m_i} * 100$$

(1)

where:

m_i= is the initial sample mass;

m_r= is the dry sample mass after the test.

CNC-based films of dimension 15 mm x 15 mm x 0.03 mm were weighed and buried into the organic substrate at 4-6 cm depth in the perforated boxes guaranteeing the aerobic conditions. The systems can be considered disintegrable according to the European standard when 90% of the plastic sample weight is lost within 90 days of analysis. In order to simulate the disintegrability in compost, a solid synthetic waste was prepared, mixing sawdust, rabbit food, compost inoculum supplied by Genesu S.p.a., starch, sugar, oil and urea. The samples tested were taken out at different times (3, 7, 21 35, 49, and 90 days), washed with distilled water and dried in an oven at 37 °C for 24 h. Fourier infrared (FT-IR) spectra of the samples in the 400–4000 cm^{-1} range, operating in ATR mode, were recorded using a Jasco FT-IR 615 spectrometer, at selected times. Thermogravimetric analysis (TGA) was performed on 10 mg samples by a Seiko Exstar 6000 TGA quartz rod microbalance. The tests were done under nitrogen

atmosphere from 25 to 900 C at 10 C/min, and the maximum degradation temperatures were considered for the different studied formulations.

Statistical analysis

The length-distribution of CNCs, ZnO, TiO_2 and Ag_2O nanoparticles have been obtained based on a count of 50 particles from different transmission electron microscopy images using Image J software. Statistical analysis was performed against neat CNC film (* for Planktonic cells, # for adherent cells) (*,# p<0,05; **, ## p<0,01; ***, ### p<0,001) using one-way analysis of variance (ANOVA). Statistical significance was established at two-tailed $p \leq 0.05$. All calculations were generated using GraphPad Prism 5.0 (GraphPad Inc., San Diego, CA).

RESULTS AND DISCUSSIONS

Material characterization

Transmission electron microscopy (TEM) has been carried out to determine the morphological features of starting raw materials. Synthesized cellulose nanocrystals shown in Figure 1a were obtained after sulphuric acid hydrolysis of commercial microcrystalline cellulose and are 172±25 nm long and ~10 nm wide. Moreover, ZnO nanoparticles were (43±24) nm long and 20 nm wide (Figure 1b), while TiO_2 and Ag_2O nanoparticles show a spherical morphology with a diameter of 12±4 nm and 270±50 nm respectively (Figure 1c and d) (statistics based on count of 50 particles).

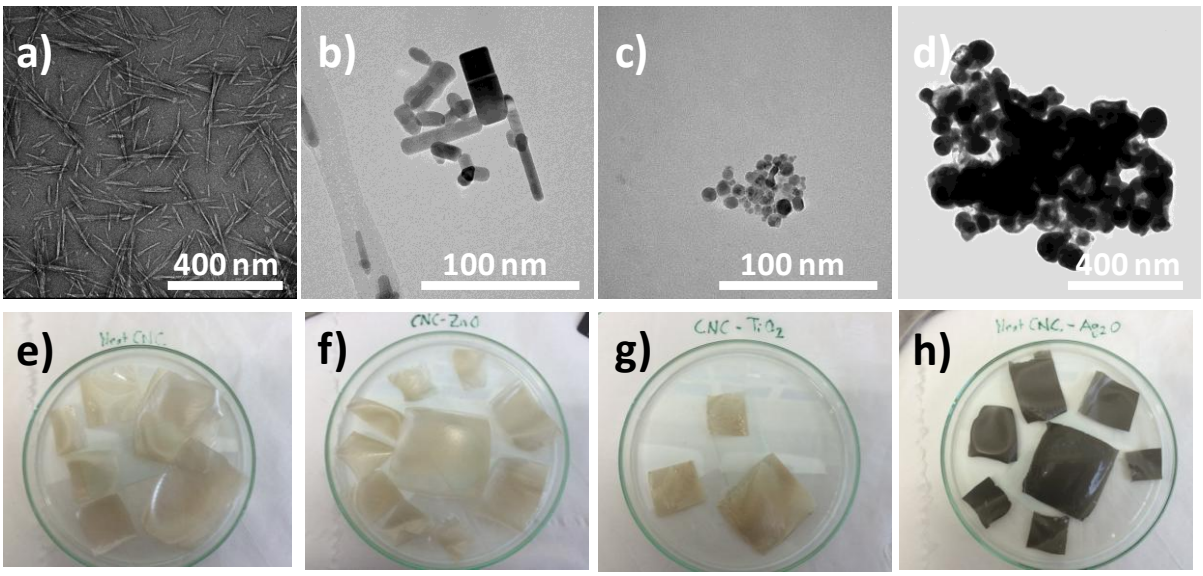

Figure. 1. First row shows the representative transmission electron microscopy (TEM) images of cellulose nanocrystals (a), ZnO (b), TiO_2 (c) and Ag_2O (d) nanoparticles. Second row displays the macroscopic appearance of synthesized films composed of CNC (e), CNC/ZnO (f), CNC/TiO_2 (g) and CNC/Ag_2O (h).

Figure 1e,f,g,h show the physical appearance of synthesized CNC, CNC/Ag_2O, CNC/ZnO and CNC/TiO_2 films. It is observed that all fabricated materials present crack-free and free-standing characteristics which optical color depends on the nature of reinforcing metal nanoparticle. Regarding the brittleness/mechanical properties of the films, it is worthy to note that, as shown in the following Figure S1, these films could be easily handled (included twisting and bending) without breaking. According to a work published by our group dealing with the same materials, the Young's modulus of these films is found in the range of 6-6.5 GPa[9]. While Ag_2O changes the transparent-like appearance of raw CNC film as a result of the strong absorbing nature of silver oxide, after ZnO and TiO_2 addition no remarkable changes in the film coloration are observed.

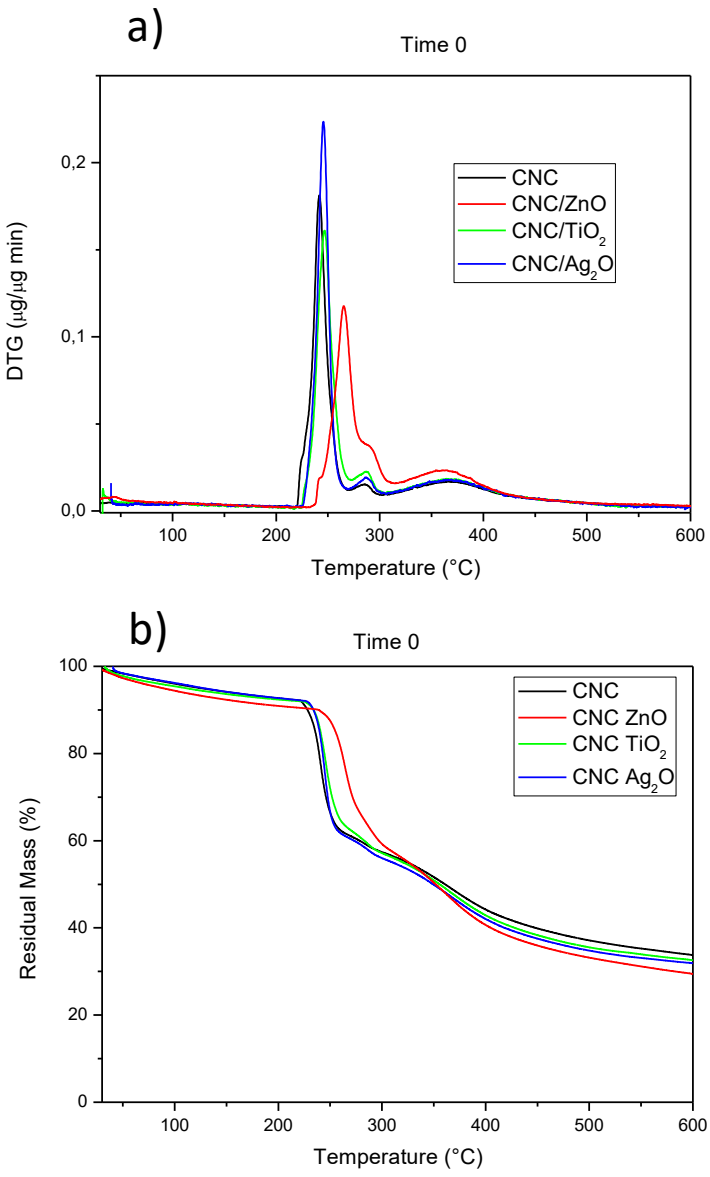

Figure. 2. TGA (a) and weight loss curves (b) of CNC and CNC nanocomposites

TGA characterization

Thermogravimetric analysis (TGA) of the CNC and CNC based nanocomposites under nitrogen atmosphere was conducted to evaluate the effect of different metal nanoparticles on the thermal stability properties of CNC based films and the results are summarized in Figure 2, showing the weight loss and derivative curves of weight loss, for different produced formulations. The curves

underline that all the produced films show a multi-step degradation behavior. The degradation step of raw CNC film begins at about 240-250 °C and reaches its maximum rate at around 260°C. This process has been previously ascribed to depolymerization, dehydration and decomposition of cellulose gyclosyl units[32].

As many inorganic materials, all the used metal particles are highly stable upon increasing temperature and they do not suffer any weight loss in the studied range. In this specific case, TiO_2 and Ag_2O nanoparticles maintain the thermal stability of CNC whereas ZnO nanoparticles are able to increase the main degradation peak of respect to raw CNC film as previously reported[33].

Microstructure and Transparency

Cross-section SEM micrographs shown in Figure 3 reveal that for all the studied systems, spindle-like CNC form a closely packed network which is arranged in a layered structure indicating that the incorporation of ZnO, TiO_2 and Ag_2O does not substantially modify the original long-range structure of CNC[29,34]. A layered structure of physically entangled cellulose nanocrystals was firstly reported in the 1990s by Revol and co-workers, which showed that the evaporation-induced self-assembly (EISA) of CNC yields a stable chiral nematic structure[35]. According to Bragg´s law, when the helical pitch of these layered materials is on the order of the wavelength of visible light, the obtained films show brilliant iridescent colors[36]. Conversely, if the helical pitch (measured as the periodic distance between adjacent layers) falls out of the 400-800 nm range, the resulting film may reflect light in the ultraviolet (UV) or infrared region, yielding optically transparent films. Since the nanocomposite films here fabricated showed a

helical pitch of about 200-230 nm as indicated by the maximum of the UV-Vis reflectance peak for neat CNC film and high-magnification SEM images in Supporting Information (Figure S2), synthesized CNC based films should present high optical transmittances in the visible region, yielding therefore transparent films. Additionally, no sign of aggregated ZnO, TiO_2 and Ag_2O nanoparticles could be observed, suggesting that they remain uniformly distributed through the nanocomposite films thanks to the electrostatic repulsion forces of CNC when dispersed in water. These forces allow obtaining more homogeneous nanocomposites than those obtained through hard-templating methods, for example, because during the co-assembly of CNC with nanoparticles, the latter remain well-distributed in solution at the molecular level[36]. These interactions allow obtaining homogeneous cellulose based nanocomposites without using complex functionalization steps which involve the use of surfactants (phosphate esters, nonylphenol, sorbitan monostearate[31,37].

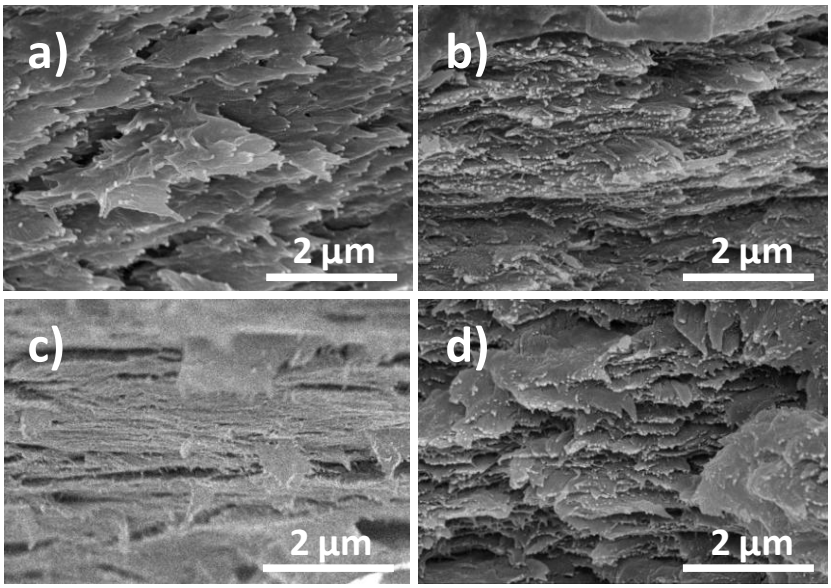

Figure. 3. SEM cross-section images of CNC (a), CNC/ZnO (b), CNC/TiO_2 (c) and CNC/Ag_2O (d) films.

According to UV-Vis spectroscopy shown in Figure 4, the optical properties of the nanocomposite films are markedly modified after the addition of metallic nanoparticles. The presence of 1 wt% of nanoparticles drastically decreases transmitted UV light (measured at 300 nm) from 19 % for neat CNC to roughly 0 % for nanocomposites[9]. The strong UV absorption of nanocomposite films is produced by the structure of reinforcing nanoparticles which present a filled valence band and an empty conduction band[38]. Moreover, while raw CNC film presents an optical transparency (determined according to the ASTM D1746-03 standard) of ~ 41 %, the transmittance in the 540-560 nm regions falls to 22 and 20 % for CNC/ZnO and CNC/TiO_2 films respectively, while CNC/Ag_2O film does not allow light to pass through in the whole UV and visible region (from 200 to 800 nm). A small reflectance peak located at 208 nm is noticed for neat CNC film. According to SEM investigations, this peak arises from the chiral structure of the films and it is not observed for reinforced films because the strong absorption of NPs in the UV region overlaps this peak[27]. The small helical pitch of few nanometers yields this reflectance peak within the UV-region in contrast to the iridescent CNC films developed by MacLachlan group, which show a intense absorption peak in the visible region[39-41]. These properties make CNC-based nanocomposite films interesting candidates for packaging applications since the UV-shielding properties of these materials may help to preserve the original properties of food by limiting the degradation reactions lipids, flavors, vitamins and pigments when exposed to light[42].

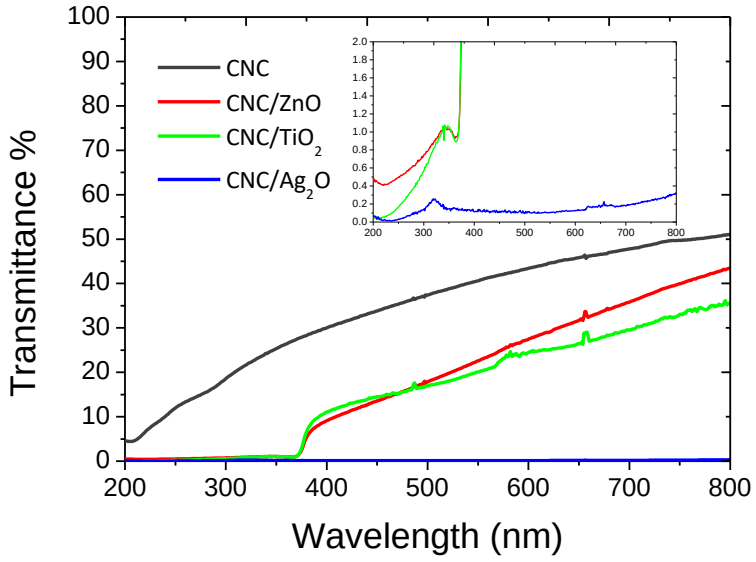

Figure. 4. UV–Vis transmittance spectra of CNC-based films.

Wettability

Surface hydrophobicity is an important parameter to take into account when exploring the material biomedical applications; furthermore the composting behavior of materials can be also affected by the wettability properties, because it may be expected that highly hydrophobic materials should present enhanced resistance against the diffusion of water through the film, which in turn may delay the degradation of CNC films during the composting process. This is of special interest in the case of cellulosic materials because of the hydrophilic nature of cellulose due to the presence of -OH groups in the basic unit of cellulose $(C_6H_{10}O_5)$[43]. In this regard, Figure 5a shows the dynamics of water contact angle (WCA) after droplet deposition. Contact angle values were determined by analyzing consecutively recorded photos over a period of 450 seconds. For the sake of clarity, representative images of a water drop at the surface of each film

are as well provided. Overall, WCA decreases over the time because water is absorbed by the CNCs as a result of the hydrophilic nature of cellulose[44]. The WCA of neat CNC at time 0 is measured to be 94º, while this value is slightly decreased to 83º and 87° for CNC/TiO_2 and CNC/Ag_2O nanocomposites. On the contrary, surface hydrophobicity of the films is markedly increased to yield a WCA of 114º after the addition of 1 wt% of ZnO as previously reported values for PLLA-based materials[13]. A careful analysis of the WCA dynamics reveals a single stage of water spreading as indicated by the linear decrease of WCA values over the studied time-frame. Once water is deposited onto the cellulosic film, it is adsorbed by the CNC network[45]. Besides of the initial WCA value which depends on the surface hydrophobicity of nanocomposite films, the adsorption dynamics are also affected by the presence of nanoparticles. The slope of WCA change has been calculated to be -0.12 º•s^{-1} for neat CNC film, while it is decreased up to -0.08 º•s^{-1} for CNC/TiO_2 film, indicating that the water adsorption of CNC films is reduced upon nanoparticle addition. We expect that these hydrophobicity differences may yield CNC films with distinctive sensitivities to compost degradation.

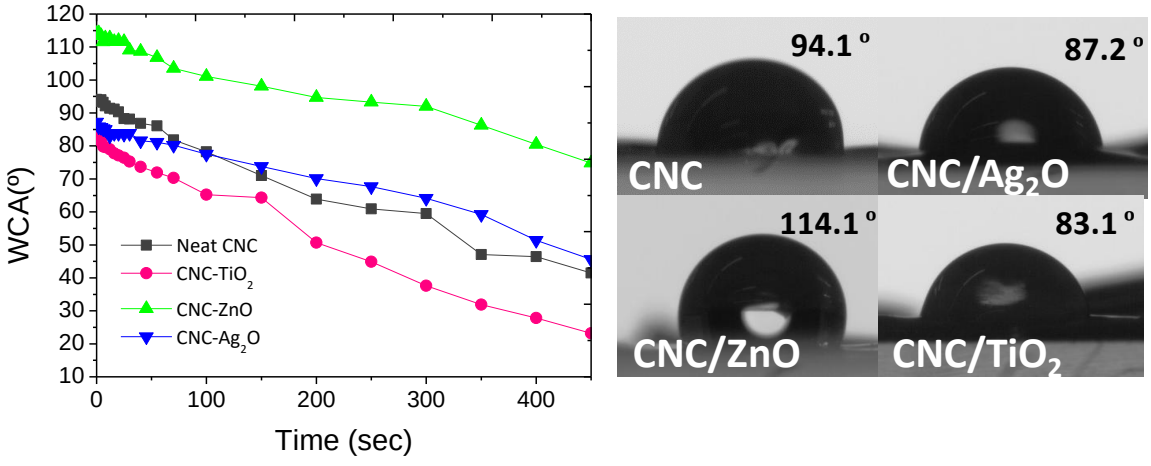

Figure. 5. WCA dynamics for CNC-based films. Representative images of a water drop at the surface of each film are provided.

Antibacterial property of CNC-based films

To investigate if the incorporation of oxide metal nanoparticles in CNC samples could exert antimicrobial activity, CNC-based films were tested against *E. coli* RB and *S. aureus* 8325-4 at both 3h and 24h, respectively (Figure 6). In particular, the antibacterial activity was evaluated both on the planktonic bacteria after being in contact with the CNC-based films or on the bacterial cells adherent to the surfaces. Differences in surviving fractions were observed based on the bacterial strains, the planktonic or adherent cells, and the incubation times.

At short incubation time (3h), the surviving fraction of *E. coli* cells adherent to the surfaces showed a significant reduction on CNC/Ag_2O ($p<0.0001$) followed by CNC/ZnO ($p<0.0001$) and, at a lesser extent, on CNC/TiO_2 (Figure 6, panel A). A similar trend was observed for the planktonic cells after being in contact with CNC-based films. Interestingly, at longer incubation time (24h), the bacterial reduction for both planktonic and adherent cells showed the trend previously observed at 3h and, in comparison to CNC, it was more noteworthy but for all the CNC-based films (Figure 6, panel B).

After 3h of incubation, the surviving fraction of *S. aureus* cells adherent to CNC-based films was significantly diminished on CNC/Ag_2O ($p<0.0001$), followed by CNC/TiO_2 ($p<0.0001$) and CNC/ZnO ($p<0.0001$) (Figure 6, panel C). The trend was completely different for the staphylococcal cells after being in contact with CNC-based films: no significant reduction following incubation with CNC/TiO_2 was observed whereas an important decrement in cell survivability ($p<0.0001$) for both CNC/Ag_2O and CNC/ZnO, even if it was less noteworthy for the ZnO nanoparticles embedded in CNC film, was detected. At 24h, the surviving fraction of the adherent cells was significantly reduced for all types of CNC-based films ($p<0.0001$) but for

the planktonic cells the results were different, being important only for CNC/Ag_2O ($p<0.05$) and CNC/TiO_2 ($p<0.005$) (Figure 6, panel D).

The antimicrobial efficacy of Ag_2O nanoparticles against *E. coli*[46] as well as against methicillin resistant *S. aureus* was already demonstrated[47]. Similarly, ZnO nanoparticles showed an antibacterial activity against Gram-positive and Gram-negative bacteria[48-50]. In our experimental conditions, the direct exposition of *E. coli* cells to CNC-based films containing Ag_2O or ZnO nanoparticles seems to be effective either at shorter and longer incubation times on both adherent and planktonic cells (with the trend Ag_2O>ZnO). The antimicrobial effect exerted by both CNC/Ag_2O and CNC/ZnO is still visible on *S. aureus* cells even if it is more significant on adherent cells at 3h in comparison to 24h. The effect of both types of CNC-based films resulted less important for planktonic staphylococcal cells at either 3 or 24h.

The effect is different when treating bacterial cells with CNC/TiO_2: the antibacterial effect is more evident at longer incubation times for adherent *E. coli* cells and vice-versa for *S. aureus* cells. TiO_2 nanoparticles have already shown toxicity toward several microorganisms and they could successfully kill numerous bacteria[51]. Interestingly, both types of cells after being in contact with CNC/TiO_2 showed higher survivability suggesting the importance of the direct contact for antibacterial activity.

So far, metal nanoparticles and oxide metal nanoparticles have been demonstrated to show antibacterial effects but the exact mechanism of their action is still being under investigation. In this regard, the mechanisms of nanomaterials against bacteria are depending on surface charge of the metal nanomaterial, shape, type and material, concentration of nanomaterial, dispersion and contact of nanomaterial to the bacterial cell, presence of active oxygen (ROS), liberation of antimicrobial ions, medium components and pH, physicochemical properties, specific surface-

area-to-volume ratios, size, role of growth rate, role of biofilm formation, cell wall of bacteria, and effect of UV illumination[49,51]. Beside all of this, our results undoubtedly seem to confirm that the incorporation of the tested types of nanoparticles in CNC films provide an effective antibacterial activity.

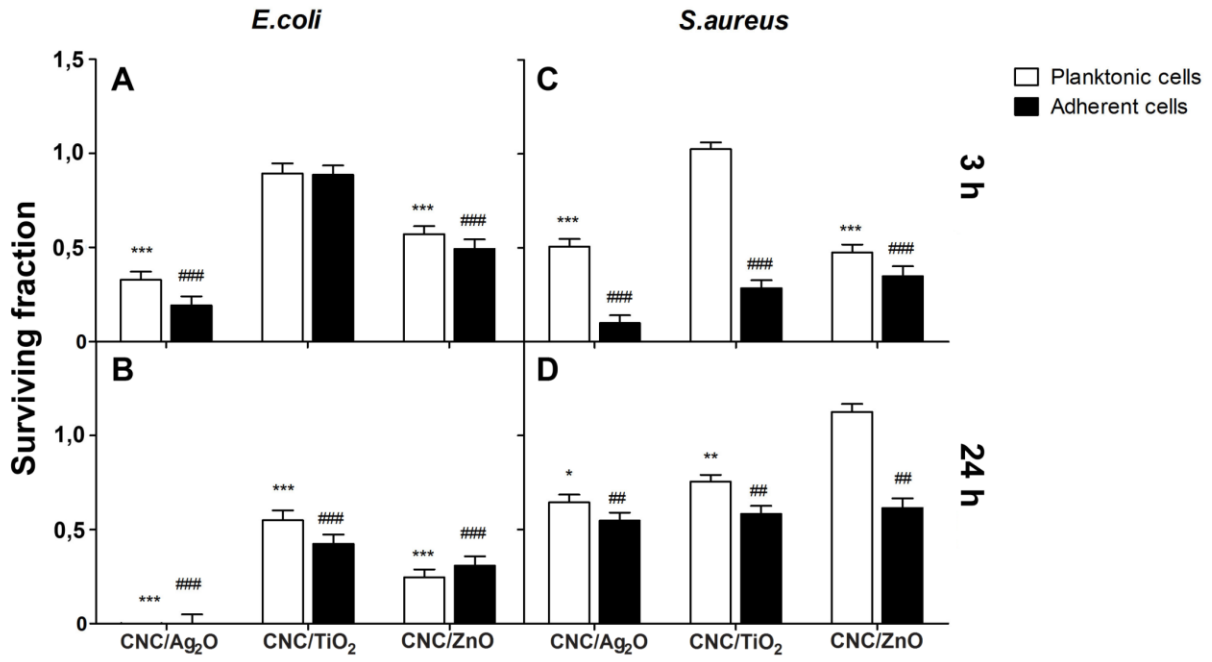

Figure. 6. The antimicrobial activity was performed on neat CNC and CNC-based films incubated with *E .coli* (panels A and B) and *S. aureus* (panels C and D) cells at 37°C for 3h (panels A and C) and 24h (panels B and D), respectively. At the indicated time points, MTT test was performed on both bacteria having being in contact with each surfaces (planktonic) or on those adherent to the CNC-based films to determine the surviving fraction. Results were normalized with TCP and expressed as ratio between bacteria either planktonic or adherent on CNC-based films and those on neat CNC. Bars indicate mean and SEM of three different experiments. Statistical analysis was performed against neat CNC film (*for Planktonic cells, # for adherent cells) (*, # $p<0,05$; **, ## $p<0,01$; ***, ### $p<0,001$).

Furthermore, to visualize the morphology of bacterial cells adherent to CNC-based films SEM studies were carried out (Figure 7). In general, the morphology of both type of bacterial cells was not modified following the direct contact with CNC-based films as documented by SEM observation at higher magnification (all the inserts of Figure 7) and comparative analysis with the control. As expected, at 24h the surfaces of the control and CNC films appeared completely covered by both types of bacterial cells whereas at 3h the number of adherent cells was less important (Figure 7, panels A and B). Again, the CNC/Ag_2O film showed the lower number of adherent cells for both type of bacterial cells at both 3h and 24h, followed by CNC/ZnO and CNC/TiO_2.

According to these results and the strong need to mitigate bacterial colonization by equipping the surfaces of biomedical devices and implants with features such as surface chemistry and surface roughness that are unfavorable for bacterial attachment, we suggest the developed materials for biomedical applications, were antibacterial performance is required, as wound healing. Despite considerable research and development efforts, the problem of infections related to biomedical devices and implants persists. Bacteria evidently can readily colonize surfaces of synthetic materials, such as those used for the fabrication of catheters, hip and knee implants, and many other devices.

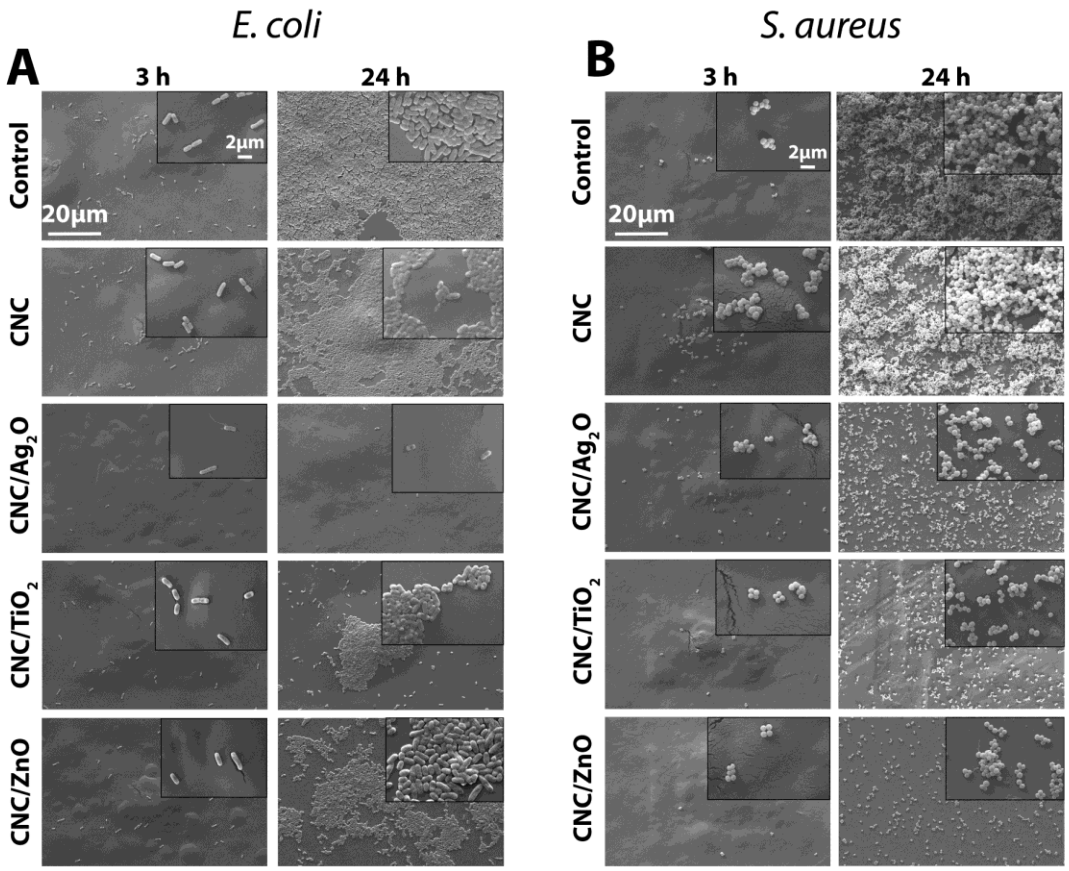

Figure. 7. Representative SEM images of adherent *E. coli* (A) and *S. aureus* (B) cells on thermanox (Ctrl), CNC, and CNC-based films incubated at 37°C for 3h and 24h, respectively. Samples for SEM observations were prepared as indicated in Materials and Methods section. Magnifications: 3000X (panel) and 10000X (insert). Scale bar: 20µm in all panels and 2µm in all inserts.

Disintegrability in composting conditions

Figure 8 shows the visual observation (Figure 8a) and the disintegrability values (Figure 8b) of CNC, CNC/ZnO, CNC/TiO_2, and CNC/Ag_2O samples taken out at different times of composting (obtained for comparison of initial weights at time 0 and final weights of the sample at the different composting times). Observing the different formulation during the first day of

incubation and until 7 days (Figure 8a), no particular alterations were detected with the exception of neat CNC film that was characterized by a browning and a deformation of the surface more evident after the 7th day in composting conditions. Moreover, the dynamics of weight loss for all CNC based films were similar to the neat CNC sample in the first part of the degradation process. Initially (after 3 days), for all the materials studied, there is an increment of the mass, that is visible in the Figure 8b as a negative weight loss, that continued, for all formulations, until 3 weeks. This effect is due to the swelling behavior of the CNC based material in humid conditions. However, opacity properties, that indicated changes of the refractive index and due to water absorption and hydrolytic degradation phenomena, started after 21 days in composting conditions,[52, 53] for all the studied formulations. Moreover, at the 21st day, fragmentation phenomena started especially for CNC/ZnO films whereas more evident fragmentation processes characterized all the studied film after 35 days in composting conditions. The results were also confirmed by the weight loss behavior since all the formulations, with the exception of CNC/Ag_2O film, reached about 50% of disintegration in 35 days. The lower disintegration rate obtained for CNC/Ag_2O that reached at least a 10% of disintegration after 90 days of incubation (90 days represents the time-limit imposed by the ISO 20200 during which the samples need to reach 90% of disintegration in order to be considered compostable in a degradation soil) was attributed to the presence of silver nanoparticles that could be able to slow and inhibit the microorganism attack due to the well know antimicrobial properties of silver. After 35 days in composting, the degradation proceeded reaching a 70% for CNC/TiO_2 and CNC/ZnO and a 60% for CNC neat film. However, although quite high levels of disintegration were reached for these three formulations, no one of the produced film reached the 90% of the disintegration representing the limit imposed by the ISO 20200. This is maybe due to the high crystalline

structure that usually characterized CNC and so, as consequence, CNC based film, able to inhibit the diffusion phenomena and to slow the disintegration process[54].

a)

b)

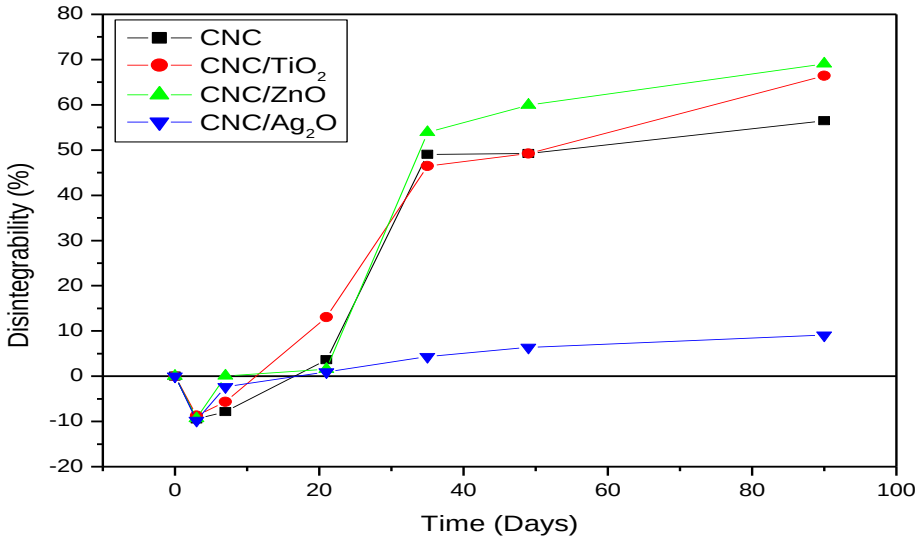

Figure. 8. Visual observation (a) and disintegrability values (b) of CNC, CNC/TiO_2, CNC/Ag_2O and CNC/ZnO samples before and after different days in composting conditions.

The behavior of the main degradation peaks of the different formulations obtained by the TGA thermograms are reported in Table 1. An increase of the maximum degradation temperatures

with the incubation times was registered for all the studied formulations until 7 days confirming previous results and due to the absorption phenomena. On the contrary, a reduction of the T_d max was registered at 21 days of incubation in composting soil that represents the kinetic inversion for the studied films and that corresponds also to the beginning of the compost maturation[55]. At this time, in fact, the samples started to change their appearance as previously discussed and some fragmentation phenomena occurred justified by this reduction in thermal stability. However, with the increase of the incubation times, all the tested samples showed an increase in the main degradation temperatures due to probably the formation a strong interaction between the OH group (probably induced by the absorption phenomena) that requires more energy to start the thermal degradation process[56].

Table 1. Main degradation temperatures for CNC, CNC/TiO_2, CNC/Ag_2O and CNC/ZnO samples before and after different days in composting conditions.

	$T_{d\ max}$(°C)						
SAMPLES	***0 Days***	***3 Days***	***7 Days***	***21 Days***	***35 Days***	***49 Days***	***90 Days***
CNC	242	261	293	228	298	293	280
CNC/TiO_2	246	290	289	278	300	317	331
CNC/ZnO	264	302	244	229	314	324	323
CNC/Ag_2O	246	282	276	225	281	278	269

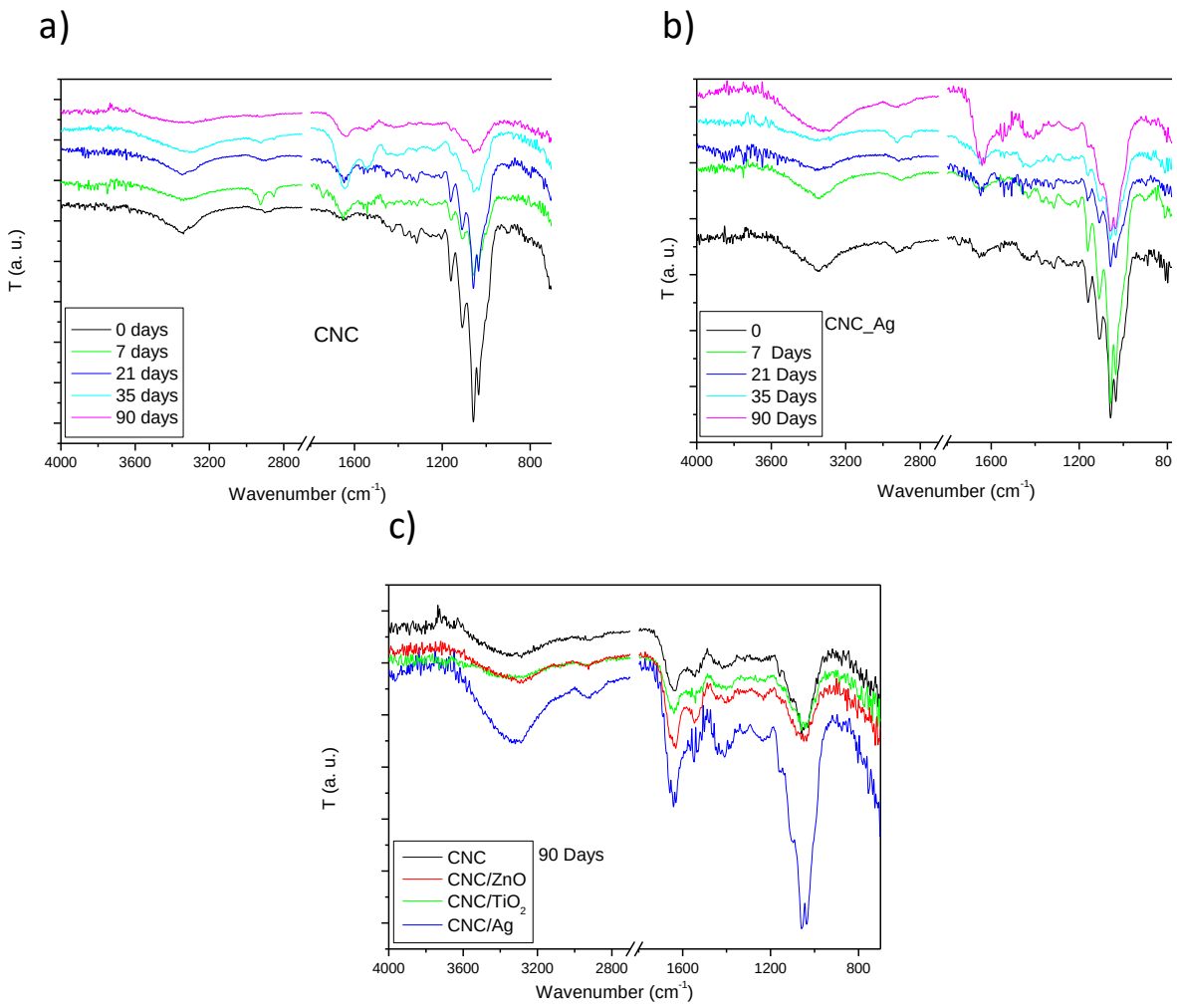

Figure. 9. Infrared spectra of CNC (a) and CNC/Ag (b) films at different incubation time and CNC nanocomposites compared to CNC films after 90 days of incubation in composting conditions (c), in the 4000-600 cm^{-1} wavenumber range .

The changes in the chemical composition of the CNC based films during disintegration in compositing conditions were explored also by using FT-IR. Figure 9a and b show the infrared spectra of CNC and CNC/Ag films at different incubation times, whereas Figure 9c shows the comparison of all the studied materials after 90 days in contact with the incubation soil, in the 4000-600 cm^{-1} wavenumber range. The decreasing of signal for the band between 1000 and1200 cm^{-1}, was evident in the CNC infrared spectra acquired during degradation in composting condition, due to the decomposition processes of organic components and that can be used to evaluate the composting processes. Meanwhile the formation of two peaks at 1540 and 1640 cm^{-1}, after 7 days of incubation was observed, due to the amide I and II, respectively. Furthermore the increasing intensity of these amide bands is evident is followed to a consequently decreasing in the main cellulose band in the 1000-1200 cm^{-1} wavenumber region.

The FT-IR results do not show any significant spectra differences between the four materials tested after 90 days of incubation. Figure 9c shows a comparison of all samples at the end of disintegration experiments. After 90 days of incubation the intensity of the band of cellulose shows similar level than the new peak in the amide region, due to decomposition process. By the analysis of the peaks is evident that the nanocomposites with silver nanoparticles show the most stable behavior, since the peak in the C-O due to CNC is the most intense. This can be due to the antibacterial effect of the silver ions that can also affect the kinetic process of the disintegration in composting conditions, as previously said. The chemistry of the nanoparticles strongly affects disintegration performance, but other environmental and nanostructural factors must be considered: the dimension, the shape, the geometry of the nanoparticles will impact the dispersion in the CNC film, that affect the rate of water penetration, as well the disintegration process in composting conditions. We think that the obtained remarkable disintegration window

of 10-70 % after 90 days for nanocomposites having only 1 wt% of nanoparticles opens new possibilities for the easy-tuning of cellulose disintegration. Furthermore parallel approaches can be followed in order to decrease the time to reach the required disintegration performance, working both on cellulose nanocrystals than nanoparticles. Some studies in fact, have been shown that the inoculation of specific microorganisms, at different phases of composting, such as bacteria and fungi, improved cellulase activities, accelerated the biodegradation of cellulose during composting process[57]

CONCLUSIONS

In the present study, we have demonstrated that CNC can be used to finely disperse functional nanoparticles, in order to successfully develop nanocomposite films with antibacterial performance with ZnO, TiO_2 or Ag_2O nanoparticles by a simple and cost-effective approach.

The results of the present work show that the chemistry, composition, the shape and the dimension of the nanoparticles introduced in CNC films at a fixed concentration affect the film appearance, microstructure, and optical properties, including thermal stability, with the nanocomposite films that exhibit the properties of both components.

This study shows the different efficacy of the tested metal oxide nanoparticles incorporated in CNC-based films against both *E. coli* and *S. aureus* strains, performed on adherent or planktonic cells after being in contact with the materials surfaces. In general, the effect was more evident on adherent *E. coli* at both 3h and 24h in comparison to *S. aureus* cells. CNC/Ag_2O films showed

the best antibacterial activity in comparison to CNC-ZnO and CNC-TiO_2 films either at shorter and longer incubation time on *E.coli* cells.

AUTHOR INFORMATION

Corresponding Authors: Erlantz Lizundia, erlantz.liizundia@ehu.eus,

Ilaria Armentano, ilaria.armentano@unitus.it.

Author Contributions

The manuscript was written through contributions of all authors. All authors have given approval to the final version of the manuscript.

ACKNOWLEDGMENT

The authors acknowledge financial Support from the Basque Country Government (IT718-13). Technical and human support provided by SGIker (UPV/EHU, MICINN, GV/EJ, EGEF and ESF) is gratefully acknowledged. This research was performed within the framework of COST Action TD1305 (Cost IPROMEDAI (Improved Protection of Medical Devices Against Infection), http://www.cost.eu/COST_Actions/tdp/TD1305).

REFERENCES

1. Campoccia, D.; Montanaro, L.; Arciola, C.R. A Review of the biomaterials technologies for infection-resistant surfaces. *Biomaterials* **2013**, *34*, 8533-8554.

2. Anselme, K.; Davidson, P.; Popa, A.M.; Giazzon, M.; Liley, M.,; Ploux L. The interaction of cells and bacteria with surfaces structured at the nanometer scale. *Acta Biomaterialia* **2010**, *6*, 3824-3846.

3. Fortunati, E.; Mattioli, S.; Visai, L.; Imbriani, M.; Fierro, J.L. F.; Kenny, J.M.; Armentano, I. Combined Effects of Ag Nanoparticles and Oxygen Plasma Treatment on PLGA Morphological, Chemical, and Antibacterial Properties. *Biomacromolecules* **2013**, *14*, 626-636.

4. Domingues, R.M.A.; Gomes, M.E.; Reis, R.L. The Potential of Cellulose Nanocrystals in Tissue Engineering Strategies. *Biomacromolecules* **2014**, *15*, 2327–2346.

5. Grishkewich, N.; Mohammed, N.; Tang, J.;Tam, K.C. Recent advances in the application of cellulose nanocrystals. *Current Opinion in Colloid & Interface Science* **2017**, *29*, 32–45.

6. Foresti, M.L.; Vázquez, A.; Boury, B. Applications of bacterial cellulose as precursor of carbon and composites with metal oxide, metal sulfide and metal nanoparticles: A review of recent advances. *Carbohydrate Polymers* **2017**, *157*, 447–467.

7. Dufresne, A. Nanocellulose: A new ageless bionanomaterial. Materials Today **2013**, *16*, 220–227.

8. Fortunati, E.; Armentano, I.; Zhou, Q.; Iannoni, A.; Saino, E.; Visai, L.; Kenny, J.M. Multifunctional bionanocomposite films of poly(lactic acid), cellulose nanocrystals and silver nanoparticles. *Carbohydrate Polymers* **2012**, *87*, 1596–1605.

9. Lizundia, E.; Urruchi, A.; Vilas, J.L.; León, L.M. Increased functional properties and thermal stability of flexible cellulose nanocrystal/ZnO films. *Carbohydrate Polymers* **2016**,

136, 250-258.

10. Habibi, Y.; Lucia, L.A.; Rojas, O.J. Cellulose nanocrystals: Chemistry, self-assembly, and applications. *Chemical Reviews* **2010**, *110*, 3479–3500.

11. Larranaga, A.; Ramos, D.; Amestoy, H.; Zuza, E.; Sarasua, J.R. Coating of bioactive glass particles with mussel-inspired polydopamine as a strategy to improve the thermal stability of poly(l-lactide)/bioactive glass composites. *RSC Advances* **2015**, *5*, 65618–65626.

12. Larrañaga, A.; Diamanti, E.; Rubio, E.; Palomares, T.; Alonso-Varona, A.; Aldazabal, P.; Martin, F.J.; Sarasua, J.R. A study of the mechanical properties and cytocompatibility of lactide and caprolactone based scaffolds filled with inorganic bioactive particles. *Materials Science and Engineering: C* **2014**, *42*, 451–460.

13. Lizundia, E.; Ruiz-Rubio, L.; Vilas J,L.; León L,M. Towards the development of eco-friendly disposable polymers: ZnO-initiated thermal and hydrolytic degradation in Poly (L-lactide)/ZnO nanocomposites. *RSC Advances* **2016**, *6*, 15660-15669.

14. Arrieta, M. P.; Fortunati, E.; Dominici, F.; López, J.; Kenny, J.M. Bionanocomposite films based on plasticized PLA-PHB/cellulose nanocrystal blends. *Carbohydrate Polymers* **2015**, *121*, 265–275.

15. Rinaldi, S.; Fortunati, E.; Taddei, M.; Kenny, J. M.; Armentano, I.; Latterini, L. Integrated PLGA-Ag nanocomposite systems to control the degradation rate and antibacterial properties. *Journal of Applied Polymer Science* **2013**, *130*, 1185–1193.

16. Tang, Y.; Hu, X.; Zhang, X.; Guo, D.; Zhang, J.; Kong, F. Chitosan/titanium dioxide nanocomposite coatings: Rheological behavior and surface application to cellulosic paper. *Carbohydrate Polymers* **2016**, *151*, 752–759.

17.Varaprasad, K.; Raghavendra, G.M.; Jayaramudu, T.; Seo, J. Nano zinc oxide-sodium

alginate antibacterial cellulose fibres. *Carbohydrate Polymers* **2016**, *135*, 349–355.

18. Dallas, P.; Sharma, V.K.; Zboril, R. Silver polymeric nanocomposites as advanced antimicrobial agents: Classification, synthetic paths, applications, and perspectives. *Advances in Colloid and Interface Science* **2011**, *166*, 199-135.

19. Panyala, N.R.; Pena-Mendez, E.M.; Havel, J. Gold and nano-gold in medicine: Overview, toxicology and perspectives. *Journal of Applied Biomedicine* **2009**, *7*, 75–91.

20. Gardner, D.J.; Oporto, G.S.; Mills, R.; Azizi Samir, M.A.S. Adhesion and surface issues in cellulose and nanocellulose. *Journal of Adhesion Science and Technology* **2008**, *22*,545–567.

21. Gunalan, S.; Sivaraj, R.; Rajendran, V. Green synthesized ZnO nanoparticles against bacterial and fungal pathogens. *Progress in Natural Science: Materials International* **2012**, 22, 693–700.

22. Ambika, S.; Sundrarajan, M. Antibacterial behaviour of Vitex negundo extract assisted ZnO nanoparticles against pathogenic bacteria. *Journal of Photochemistry and Photobiology B: Biology* **2015**, *146*, 52–57.

23. Lukach, A.; Thérien-Aubin, H.; Querejeta-Fernández, A.; Pitch, N.; Chauve, G.; Méthot, M.; Bouchard, J.; Kumacheva, E. Coassembly of Gold Nanoparticles and Cellulose Nanocrystals in Composite Films. *Langmuir* **2015**, *31*, 5033−5041

24. Ifuku, S.; Tsuji, M.; Morimoto, M.; Saimoto, H.; & Yano, H. Synthesis of silver nanoparticles templated by TEMPO-mediated oxidized bacterial cellulose nanofibers. *Biomacromolecules* **2009**, *10*, 2714–2717.

25. Lizundia, E., Meaurio, E., & Vilas, J. L. In *Multifunctional Polymeric Nanocomposites Based on Cellulosic Reinforcements*. Chapter 3 - Grafting of Cellulose Nanocrystals, **2016***;*

61–113.

26. Zhang, W.; Liang, Y.; Luo, W.; Fang, Y. Effects of clay-modifying agents on the morphology and properties of poly(methyl methacrylate)/clay nanocomposites synthesized via X-ray irradiation polymerization. *Journal of Polymer Science Part A: Polymer Chemistry* **2003**, *41*, 3218–3226.

27. Lizundia, E.; Nguyen, T.D.; Vilas, J.L.; Hamad, W.Y.; MacLachlan, M.J. Chiroptical luminescent nanostructured cellulose films. *Materials Chemistry Frontiers* **2017**, *1*, 979-987.

28. Lizundia, E.; Vilas, J.L.; León, L.M. Crystallization, structural relaxation and thermal degradation in Poly(l-lactide)/cellulose nanocrystal renewable nanocomposites. *Carbohydrate Polymers* 2015, 123, 256-265.

29. Yalcinkaya, E.E.; Puglia, D.; Fortunati, E.; Bertoglio, F.; Bruni, G.; Visai, L.; Kenny, J.M. Cellulose nanocrystals as templates for cetyltrimethylammonium bromide mediated synthesis of Ag nanoparticles and their novel use in PLA films. *Carbohydrate Polymer* **2017**, *157*, 1557-1567.

30. Bari, A.; Bloise, N.; Fiorilli, S.; Novajra, G.; Vallet-Regí, M.; Bruni, G.; Torres-Pardo, A.; González-Calbet, J.M.; Visai, L.; Vitale-Brovarone, C. Copper-containing mesoporous bioactive glass nanoparticles as multifunctional agent for bone regeneration. *Acta Biomater* **2017**, *55*, 493–504.

31. Fortunati, E.; Mattioli, S.; Armentano, I.; Kenny, J.M. Spin coated cellulose nanocrystal/silver nanoparticle films. *Carbohydrate Polymers* **2014**, *113*, 394–402.

32. Roman, M.; Winter, W.T. Effect of sulfate groups from sulfuric acidhydrolysis on the thermal degradation behaviour of bacterial cellulose. *Biomacromolecules* **2004**, *5*, 1671–1677.

33. Goikuria, U.; Larrañaga, A.; Vilas, J.L.; Lizundia, E. Thermal stability increase in metallic nanoparticles-loaded cellulose nanocrystal nanocomposites, *Carbohydrate Polymers* **2017**, *171*, 193-201.

34. Revol, J.F.; Bradford, H.; Giasson, J.; Marchessault, R.H.; Gray, D.G. Helicoidal self-ordering of cellulose microfibrils in aqueous suspension. *International Journal of Biological Macromolecules* **1992**, *14*, 170–172.

35. Kelly, J.A.; Giese, M.; Shopsowitz, K.E.; Hamad, W.Y.; MacLachlan, M. J. The development of chiral nematic mesoporous materials. *Accounts of Chemical Research* **2014**, *47*, 1088–1096.

36. Xu, J.; Nguyen, T.-D.; Xie, K.; Hamad, W.Y.; MacLachlan, M.J. Chiral nematic porous germania and germanium/carbon films. *Nanoscale* **2015**, *7*, 13215–13223.

37. Kim, J.; Montero, G.; Habibi, Y.; Hinestroza, J.P.; Genzer, J.; Argyropoulos, D.S.; Rojas, O.J. Dispersion of cellulose crystallites by nonionic surfactants in a hydrophobic polymer matrix. *Polymer Engineering and Science* **2009**, *49*, 2054–2061.

38. Kubacka, A.; Fernández-García, M.; Colón, G. Advanced nanoarchitectures for solar photocatalytic applications. *Chemical Reviews* **2012**, *112*, 1555-1614.

39. Giese, M.; Blusch, L.K.; Khan, M.K.; MacLachlan, M.J. Functional materials from cellulose-derived liquid-crystal templates. *Angewandte Chemie (International Ed. in English)* **2015**, *54*, 2888–910.

40. Schlesinger, M.; Hamad, W.Y.; Maclachlan, M.J. Optically tunable chiral nematic mesoporous cellulose films. *Soft Matter* **2015**, *15*, 4686–4694.

41. Shopsowitz, K.E.; Qi, H.; Hamad, W.Y.; Maclachlan, M.J. Free-standing mesoporous silica films with tunable chiral nematic structures. *Nature* **2010**, *468*, 422–425.

42. Silvestre, C.; Duraccio, D.; Cimmino, S. Food packaging based on polymer nanomaterials. *Progress in Polymer Science (Oxford)* **2011**, *36*, 1766–1782.

43. Khwaldia, K.; Arab-Tehrany, E.; Desobry, S. Biopolymer Coatings on Paper Packaging Materials. *Comprehensive Reviews in Food Science and Food Safety* **2010**, *9*, 82-91.

44. Gao, Z.; Zhai, X.; Liu, F.; Zhang, M.; Zang, D.; & Wang, C. Fabrication of TiO_2/EP super-hydrophobic thin film on filter paper surface. *Carbohydrate Polymers* **2015,** *128*, 24–31.

45. Tammelin, T.; Abburi, R.; Gestranius, M.; Laine, C.; Setälä, H.; Österberg, M. Correlation between cellulose thin film supramolecular structures and interactions with water. *Soft Matter*, **2015**, 11: 4273-4282.

46. Sondi, I.; Salopek-Sondi, B. Silver nanoparticles as antimicrobial agent: a case study on E. coli as amodel for Gram-negative bacteria. *J. Colloid Interface Sci.* **2004**, *275*, 177–182.

47. Sangappa, M.; Thiagarajan, P. Combating drug resistant pathogenic bacteria isolated from clinical infections, with silver oxide nanoparticles. *Indian J Pharm Sci.* **2015**, *77*, 151-155.

48. Azam, A.; Ahmed, A.S.; Oves, M.; Khan, M.S.; Habib, S.S.; Memic, A. Antimicrobial activity of metal oxide nanoparticles against Gram-positive and Gram-negative bacteria:a comparative study. *Int. J. Nanomedicine* **2011**, *7*, 6003–6009.

49. Dizaj, S.M.; Lotfipour, F.; Barzegar-Jalali, M.; Zarrintan, M.H.; Adibkia, K. Antimicrobial activity of the metals and metal oxide nanoparticles. *Mater Sci Eng C Mater Biol Appl.* **2014**, *44*, 278-84.

50. Emami-Karvani, Z.; Chehrazi, P. Antibacterial activity of ZnO nanoparticle on Gram positive and gram-negative bacteria. *Afr. J. Microbiol. Res.* **2011**, *5*, 1368–1373.

51. Hoseinzadeh, E.; Makhdoumi, P.; Taha, P.; Stelling, J.; Hossini, H.; Kamal, M.A.; Ashraf, G.M. A review on nano-antimicrobials: metal nanoparticles, methods, and mechanisms. *Curr Drug Metab*. **2017**, *18*, 120-128.

52. Bitinis, N.; Fortunati, E.; Verdejo, R.; Bras, J.; Kenny, J.M.; Torre L, et al. Poly(lactic acid)/natural rubber/cellulose nanocrystal bionanocomposites Part II. Properties evaluation. *Carbohydrate Polymer* **2013**, *96*, 621–7.

53. Fukushima, K.; Tabuani, D.; Abbate, C.; Arena, M.; Ferreri, L. Effect of sepiolite on the biodegradation of poly(lactic acid) and polycaprolactone. *Polymer Degradation Stability* **2010**, *95*, 2049–56.

54. Fortunati, E.; Peltzer, M.; Armentano, I.; Torre, L.; Jimenez, A.; Kenny, J.M. Effects of modified cellulose nanocrystals on the barrier and migration properties of PLA nano-biocomposites. *Carbohydrate Polymer* **2012**, *90*, 948–56.

55. Luzi, F.; Fortunati, E.; Jimenez, A.; Puglia, D.; Pezzolla, D.; Gigliotti, G.; Kenny, J.M.; Chiralt, A.; Torre, L. Production and characterization of PLA_PBS biodegradable blends reinforced with cellulose nanocrystals extracted from hemp fibres. *Industrial Crops and Products* **2016**, *93*, 276–289.

56. Luzi, F.; Fortunati, E.; Giovanale, G.; Mazzaglia, A.; Torre, L.; Balestra, G.M.; Cellulose nanocrystals from Actinidia deliciosa pruning residues combined with carvacrol in PVA_CH films with antioxidant/antimicrobial properties for packaging applications. *International Journal of Biological Macromolecules* **2017**, *104*: Part A-43–55.

57. Zhao, Y.; Zhao, Y.; Zhang, Z.; Wei, Y.; Wang H.; Lu, Q.; Li, Y.; Wei, Z. Effect of thermo-tolerant actinomycetes inoculation on cellulose degradation and the formation of humic substances during composting. *Waste Management* **2017**, *68*: 64-73.